

# Improving the accuracy of the neuroevolution machine learning potential for multi-component systems

Zheyong Fan<sup>1,\*</sup>

<sup>1</sup>College of Physical Science and Technology, Bohai University, Jinzhou 121013, P. R. China  
(Dated: January 25, 2022)

In a previous paper [Fan Z *et al.* 2021 Phys. Rev. B, **104**, 104309], we developed the neuroevolution potential (NEP), a framework of training neural network based machine-learning potentials using a natural evolution strategy and performing molecular dynamics (MD) simulations using the trained potentials. The atom-environment descriptor in NEP was constructed based on a set of radial and angular functions. For multi-component systems, all the radial functions between two atoms are multiplied by some fixed factors that depend on the types of the two atoms only. In this paper, we introduce an improved descriptor for multi-component systems, in which different radial functions are multiplied by different factors that are also optimized during the training process, and show that it can significantly improve the regression accuracy without increasing the computational cost in MD simulations.

## I. INTRODUCTION

In recent years, machine-learning (ML) potentials [1–5] have played an important role in molecular dynamics (MD) simulations. A well trained ML potential can achieve an accuracy close to that of the training data and a speed that cannot be achieved by *ab initio* MD simulations. After the pioneering work by Behler and Parrinello [6] on the high-dimensional neural network (NN) potential, other alternatives such as the Gaussian approximation potential (GAP) [7] and some linear regression ML potentials [8, 9] were also developed. Many methods and computer codes for constructing NN potentials have been developed by exploring standard ML libraries [10–18].

Recently, the present author developed a framework called neuroevolution potential (NEP) [19] for training NN-based ML potential using a natural evolution strategy [20, 21], instead of the conventional back propagation (gradient descent) approach. NEP has been implemented in version 2.6 of the open-source GPUMD package [22–24]. It has been demonstrated [19] that NEP as implemented in GPUMD can achieve an accuracy comparable to other popular implementations of ML potentials [10, 25, 26], while exhibiting a much higher computational efficiency in MD simulations.

In this paper, we show that for multi-component systems, i.e., systems with multiple atom types, the accuracy of NEP can be significantly improved. We present the improved approach and implement it version 2.9 of GPUMD. For simplicity, the NEPs as implemented in versions 2.6 and 2.9 of GPUMD will be called NEP1 and NEP2, respectively. We will use bulk PbTe and Al-Cu-Mg alloy as case studies to show the improved accuracy of NEP2 as compared to NEP1.

## II. THEORY

### A. The previous NEP1

The ML potential in NEP1 [19] is a local many-body one, where “local” means that the total potential energy  $U$  of a system of  $N$  atoms can be written as a sum of site energies,  $U = \sum_{i=1}^N U_i$ . The site energy  $U_i$  of atom  $i$  is taken as a function of a set of  $N_{\text{des}}$  descriptor components  $\{q_\nu^i\}_{\nu=1}^{N_{\text{des}}}$ . The function is taken as a NN with a single hidden layer with  $N_{\text{neu}}$  neurons:

$$U_i = \sum_{\mu=1}^{N_{\text{neu}}} w_\mu^{(2)} \tanh \left( \sum_{\nu=1}^{N_{\text{des}}} w_{\mu\nu}^{(1)} q_\nu^i - b_\mu^{(1)} \right) - b^{(2)}, \quad (1)$$

where  $w_{\mu\nu}^{(1)}$ ,  $w_\mu^{(2)}$ ,  $b_\mu^{(1)}$ , and  $b^{(2)}$  are the trainable weight and bias parameters in the NN.

For a central atom  $i$ , there is a set of radial descriptor components ( $0 \leq n \leq n_{\text{max}}^{\text{R}}$ ),

$$q_n^i = \sum_{j \neq i} g_n(r_{ij}), \quad (2)$$

and a set of angular descriptor components ( $0 \leq n \leq n_{\text{max}}^{\text{A}}$  and  $1 \leq l \leq l_{\text{max}}$ ),

$$q_{nl}^i = \sum_{j \neq i} \sum_{k \neq i} g_n(r_{ij}) g_n(r_{ik}) P_l(\cos \theta_{ijk}), \quad (3)$$

where  $P_l(\cos \theta_{ijk})$  is the Legendre polynomial of order  $l$ ,  $\theta_{ijk}$  being the angle formed by the  $ij$  and  $ik$  bonds. The functions  $g_n(r_{ij})$  are radial functions and they are defined as

$$g_n(r_{ij}) = \frac{T_n \left( 2 \left( \frac{r_{ij}}{r_c} - 1 \right)^2 - 1 \right) + 1}{2} f_c(r_{ij}) c_{ij}. \quad (4)$$

Here  $T_n(x)$  is the  $n$ -th order Chebyshev polynomial of the first kind and  $f_c(r_{ij})$  is the cutoff function defined as

$$f_c(r_{ij}) = \frac{1}{2} \left( 1 + \cos \left( \pi \frac{r_{ij}}{r_c} \right) \right) \quad (5)$$

\* brucenju@gmail.com

for  $r \leq r_c$  and  $f_c(r_{ij}) = 0$  for  $r > r_c$ . The cutoff radius  $r_c$  can take different values for the radial and angular components, which are denoted as  $r_c^R$  and  $r_c^A$ , respectively.

Following Refs. 27 and 28, a factor  $c_{ij}$  is included in the definition of the radial functions  $g_n(r_{ij})$  to account for the different atom types. Gastegger *et al.* [27] suggested to use  $c_{ij} = z_j$ , where  $z_j$  is the atomic number of atom  $j$  and Artrith *et al.* [28] suggested to use  $c_{ij} = \pm 1, \pm 2, \dots$ . In NEP1,  $c_{ij}$  is chosen as  $\sqrt{z_i z_j}$ .

## B. The improved NEP2

It is clear that in all the schemes above, the resulting descriptor has the permutation symmetry, i.e., the descriptor is invariant upon a permutation of the atoms with the same type. However, hand-chosen values for  $c_{ij}$  might not be optimal. More importantly, the coefficients  $c_{ij}$  are the same for all the radial functions  $g_n(r_{ij})$ , which do not depend on  $n$ . In NEP2, we propose to make these coefficients  $n$ -dependent, leading to the following radial functions:

$$g_n(r_{ij}) = \frac{T_n \left( 2 \left( \frac{r_{ij}}{r_c} - 1 \right)^2 - 1 \right) + 1}{2} f_c(r_{ij}) c_{nij}. \quad (6)$$

If the considered material has  $N_{\text{typ}}$  atom types, the number of  $c_{nij}$  coefficients is

$$N_{\text{typ}}^2 (n_{\text{max}}^R + n_{\text{max}}^A + 2). \quad (7)$$

The factor  $N_{\text{typ}}^2$  enumerates all the possible ordered combinations of atom types: both atoms  $i$  and  $j$  can be one of the  $N_{\text{typ}}$  types. Therefore, for a given  $n$ , there are  $N_{\text{typ}}^2$  possible  $c_{nij}$  values. Taking  $N_{\text{typ}} = 3$  as an explicit example and denoting the atom types as  $a$ ,  $b$ , and  $c$ , we have the following  $N_{\text{typ}}^2 = 9$  coefficients for a given  $n$ :  $c_{naa}$ ,  $c_{nab}$ ,  $c_{nac}$ ,  $c_{nba}$ ,  $c_{nbb}$ ,  $c_{nbc}$ ,  $c_{nca}$ ,  $c_{ncb}$ , and  $c_{ncc}$ ; there will be  $9(n_{\text{max}}^R + n_{\text{max}}^A + 2)$  parameters in total. These  $c_{nij}$  parameters are not hand chosen, but are taken as free parameters to be optimized during the training process, similar to the weight and bias parameters in the NN. One difference between the  $c_{nij}$  parameters and the NN parameters is that we require that

$$|c_{nij}| \geq \frac{1}{10}. \quad (8)$$

The purpose of applying this restriction is to avoid too small values for the descriptor components.

The method can also be applied to neural network potentials trained using the back propagation method, but one needs to compute the derivatives of a loss function with respect to the extra parameters introduced into the descriptor. By contrast, the introduction of these parameters adds little extra work in our approach as the natural evolution strategy does not require the calculation of the derivative of the loss function with respect to

any parameter. This is one of the advantages of the natural evolution strategy compared to back propagation. In the moment tensor potential (MTP) [29], similar optimization of some radial coefficients has been used for multi-component systems. In the recursively embedded-atom NN potential [18], these coefficients for a central atom  $i$  are considered to be recursively dependent on the descriptors of the neighbor atoms  $j$  through extra NNs.

We stress that the introduction of more parameters to the radial functions does not add more computations to the ML potential, as the number of descriptor components and the number of NN parameters, which affect the speed of the potential in MD simulations, are not changed. With this in mind, we next evaluate the regression accuracy of NEP2 as compared to NEP1.

## III. RESULTS AND DISCUSSION

### A. Bulk PbTe

We first use the training data set of bulk PbTe as studied in Ref. 19 to compare NEP1 and NEP2. There are 325 structures, each with 250 atoms. The training data set and related inputs and outputs are available from a public Gitlab repository [30]. All the relevant hyperparameters are the same for NEP1 and NEP2 and are listed in Table I.

TABLE I. The hyperparameters used in the NEP potential for the two materials, bulk PbTe and Al-Cu-Mg alloy. Here,  $r_c^R$  ( $r_c^A$ ) is the cutoff radius for the radial (angular) components of the descriptor,  $n_{\text{max}}^R$  ( $n_{\text{max}}^A$ ) is the Chebyshev polynomial expansion order for the radial (angular) components,  $l_{\text{max}}$  is the Legendre polynomial expansion order for the angular components,  $N_{\text{neu}}$  is the number of neurons in the hidden layer of the neural network,  $\lambda_1$  ( $\lambda_2$ ) is the  $\mathcal{L}_1$  ( $\mathcal{L}_2$ ) regularization parameter,  $N_{\text{bat}}$  is the batch size (number of structures used within one generation).  $N_{\text{pop}}$  is the population size in the natural evolution strategy algorithm, and  $N_{\text{gen}}$  is the maximum number of generations to be evolved. The training time using one GeForce RTX 2080ti GPU is also provided.

Parameter	PbTe	Al-Cu-Mg alloy
$r_c^R$	8 Å	6 Å
$r_c^A$	4 Å	4 Å
$n_{\text{max}}^R$	12	15
$n_{\text{max}}^A$	6	10
$l_{\text{max}}$	4	4
$N_{\text{neu}}$	40	40
$\lambda_1$	0.05	0.05
$\lambda_2$	0.05	0.05
$N_{\text{bat}}$	25	1000
$N_{\text{pop}}$	50	50
$N_{\text{gen}}$	$10^5$	$10^5$
Training time	1 hour	7 hours

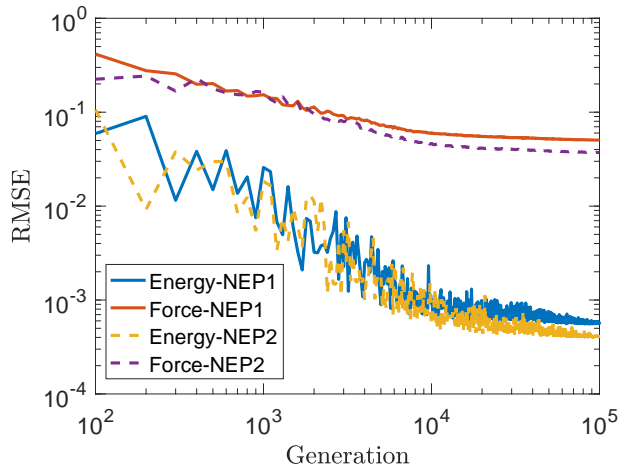


FIG. 1. Evolution of the energy and force RMSEs for bulk PbTe during the training process for NEP1 (solid lines) and NEP2 (dashed lines).

Figure 1 shows the evolution of the root mean square errors (RMSEs) of energy and force as obtained by NEP1 and NEP2 with respect to the generation in the natural evolution strategy. The total number of generations is chosen as  $10^5$  here, which is large enough to achieve convergence of the RMSEs. Within the first few thousand generations, the RMSEs are comparable between NEP1 and NEP2. However, NEP2 develops smaller RMSEs afterwards. Up to  $10^5$  generations, the energy and force RMSEs obtained in NEP1 are 0.56 meV/atom and 50 meV/Å respectively. The corresponding values obtained in NEP2 are 0.39 meV/atom and 38 meV/Å. The reduction of regression errors is about 30% for both energy and force. For completeness, we list the RMSEs and mean absolute errors (MAEs) of all the relevant potentials in Table II.

TABLE II. Accuracy comparison between NEP1 and NEP2. Energy and virial errors are in units of meV/atom, and force error is in units of meV/Å.

Material	Accuracy	NEP1	NEP2
Bulk PbTe	Energy RMSE	0.56	0.39
	Energy MAE	0.37	0.29
	Force RMSE	50	38
	Force MAE	36	28
Al-Cu-Mg alloy	Energy RMSE	510	11
	Energy MAE	410	7.3
	Force RMSE	400	72
	Force MAE	260	50
	Virial RMSE	330	43
	Virial MAE	190	27

Figure 2 compares the predicted energies by NEP1 and

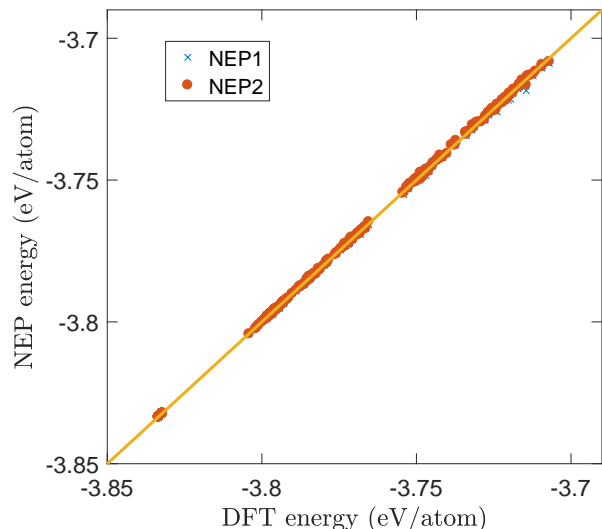


FIG. 2. Energy as calculated from NEP1 and NEP2 for bulk PbTe compared with the training data from quantum mechanical DFT calculations. The solid line represents the identity function used to guide the eyes.

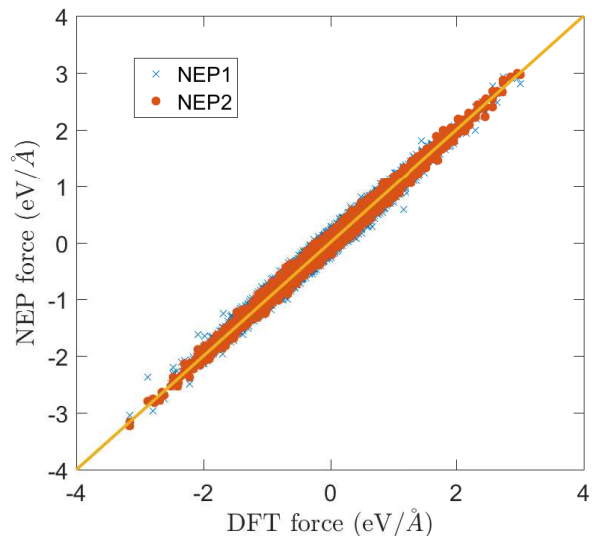


FIG. 3. Force as calculated from NEP1 and NEP2 for bulk PbTe compared with the training data from quantum mechanical DFT calculations. The solid line represents the identity function used to guide the eyes.

NEP2 and those from quantum mechanical density functional theory (DFT) calculations. Figure 3 shows similar results for force. It can be seen that the energy and force errors from NEP2 are indeed smaller than those from NEP1. Particularly, in NEP1, there are some force errors larger than 0.5 eV/Å, which are absent from NEP2.

To better appreciate the performance of NEP2, we

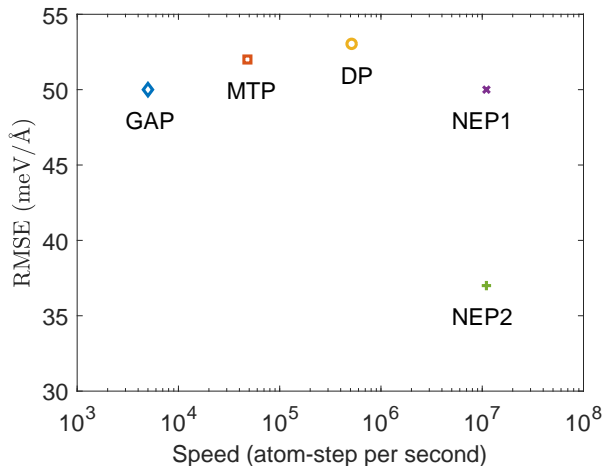


FIG. 4. Force RMSE and MD speed for the various ML potentials trained using the same set of training data for PbTe. The results for NEP1, GAP, MTP and DP are taken from Ref. 19. For GAP and MTP, 72 Intel Xeon-Gold 6240 CPU cores are used; for DP and NEP (both NEP1 and NEP2), one Nvidia Tesla V100 GPU card is used. These CPU and GPU resources are of comparable price.

compare it with both NEP1 and some other popular ML potential packages [10, 25, 26]. Figure 4 shows the force regression accuracy and MD speed for NEP1, NEP2, GAP [25], MTP [26], and DP (deep potential) [10]. The MD speed is measured as the product of the number of atoms and the number of steps that can be achieved per second. We see that NEP1 is already of comparable accuracy to the other ML potentials in this case, and is one to three orders of magnitude faster. NEP2 can achieve a higher accuracy than NEP1 while keeping the speed of NEP1. Therefore, NEP2 can achieve a high accuracy and a high computational speed simultaneously.

To make sure that the high accuracy of NEP2 is not a result of overfitting, we perform MD simulations to calculate the thermal conductivity of PbTe from 300 K to 700 K. We use the efficient homogeneous nonequilibrium MD (HNEMD) method [19, 33] with a driving force parameter of  $1.0 \mu\text{m}^{-1}$ . We use a cubic simulation cell of 8000 atoms and a time step of 1.0 fs. For each temperature, three independent HNEMD simulations are performed, each with a production time of 2000 ps. In Fig. 5, we compare the thermal conductivity values calculated from NEP1 and NEP2 and experimental ones [31, 32]. While the two sets of experimental data have some discrepancies, it can be seen that the lattice thermal conductivity values calculated using NEP2 do not give a worse agreement with the experimental ones than NEP1. This indicates that the high accuracy of NEP2 is not a result of overfitting.

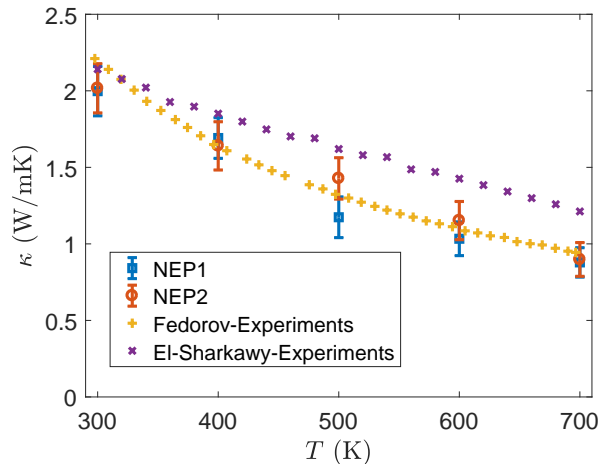


FIG. 5. Lattice thermal conductivity of bulk PbTe as a function of temperature from HNEMD simulations with NEP1 and NEP2 and from experiments [31, 32]. The NEP1 results are taken from Ref. 19.

## B. Al-Cu-Mg alloy

We now move from the relatively simple case of bulk PbTe to the more challenging case of Al-Cu-Mg alloy as studied by Jiang *et al.* [34] using the DeePMD-kit package [10]. A large data set with a full range of relative concentrations of the three atom types has been generated using a concurrent-learning scheme [34]. There are 141409 structures with more than three million atoms in total. We randomly select  $10^4$  structures as the testing set and use the remaining structures for training. The hyperparameters we use for NEP1 and NEP2 are listed in Table I.

Figures 6(a)-(c) show the energy, force, and virial as calculated from NEP1 and NEP2 compared with the DFT training data. We see that NEP1 has very large errors in all the quantities, while NEP2 has much higher accuracy (See Table II for the RMSE and MAE values). Figure 6(d) shows the MD simulation speed of NEP2 as a function of the number of atoms in the simulated system (NEP1 is unstable and we thus have not run MD simulations with it). Using a single Tesla A100 GPU (with 80 GB device memory), we can run MD simulations with systems containing up to about 7 million atoms and the computational speed is over  $1.5 \times 10^7$  atom-step/second. As a reference, we note that the Al-Cu-Mg DP potential after model compression [35] can run MD simulations with systems containing up to about 60 thousand atoms with a computational speed of about  $1.9 \times 10^5$  atom-step/second using one Tesla V100 GPU (with 32 GB device memory).

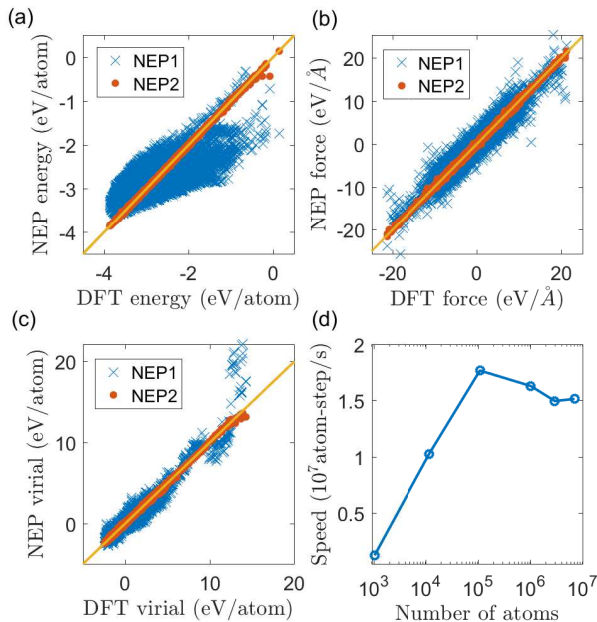


FIG. 6. (a) Energy, (b) force, and (c) virial as calculated from NEP1 and NEP2 for the Al-Cu-Mg testing data set compared with the DFT training data. The solid lines represent the identity function used to guide the eyes. (d) Computational speed of the NEP2 potential as a function of the number of atoms using one Tesla A100 GPU card.

### C. Origin of the higher accuracy of NEP2 as compared to NEP1

To understand the origin of the higher accuracy achievable by NEP2 as compared to NEP1, we examine the distributions of some descriptor components in Fig. 7 and Fig. 8. For the radial components ( $q_n$  with  $n = 1$  to  $n = 6$ ) shown in Fig. 7, the distributions for Pb and Te atoms are well distinguishable in both NEP1 and NEP2. However, for the angular components ( $q_{n4}$  with  $n = 1$  to  $n = 6$ ) shown in Fig. 8, the distributions for Pb and Te atoms are almost identical in NEP1 but are well distinguishable in NEP2. The fact that the angular descriptor distributions for Pb and Te atoms are almost identical in NEP1 is related to the choice of  $c_{ij} = \sqrt{z_i z_j}$  in Eq. (4) and the relatively small cutoff for the angular components. In NEP2, without increasing the cutoff for the angular components but simply optimizing the  $c_{nij}$  parameters in Eq. (6) for each radial function  $g_n$  can lead to more distinguishable descriptor distributions for different atom types hence better discrimination of the different atom types in a multi-component system. This is the origin of the higher accuracy of NEP2 as compared to NEP1.

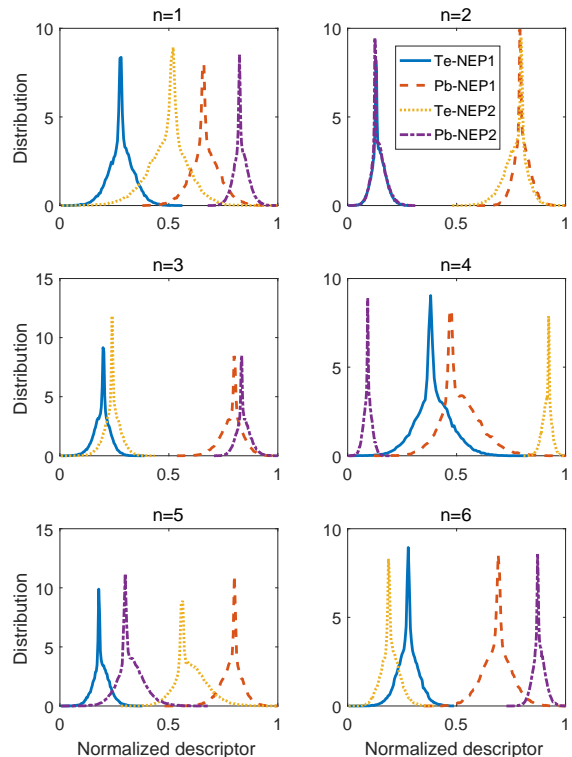


FIG. 7. Distribution of the normalized radial descriptor components  $\{q_n\}_{n=1}^6$  for the Pb and Te atoms in NEP1 and NEP2.

## IV. SUMMARY AND CONCLUSIONS

In summary, we have proposed an improved scheme of considering different atom types in the atom-environment descriptor used in the neuroevolution machine-learning potential. The improved method leads to higher regression accuracy without increasing the computational cost in molecular dynamics simulations, as demonstrated using two case studies: bulk PbTe and Al-Cu-Mg alloy. The increased regression accuracy is shown to originate from the improved discrimination of the descriptor distributions for the different atom types in the multi-component system. This improved neuroevolution machine-learning potential is implemented in version 2.9 of the open-source GPUMD package.

## ACKNOWLEDGMENTS

We thank Haikuan Dong, Jiahui Liu, Keke Song, Yanzhou Wang, Ke Xu, Penghua Ying, Zezhu Zeng, and many other GPUMD users for testing the versions developed during the course of this research. ZF acknowledges the supports from the National Natural Science Foundation of China (NSFC) (No. 11974059) and the Sci-



ence Foundation from Education Department of Liaoning Province under Grant No. LQ2019010.

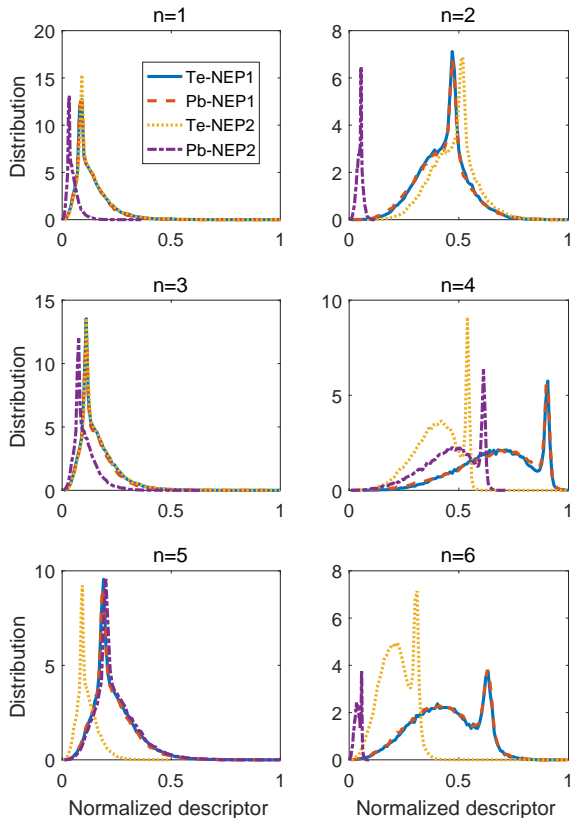


FIG. 8. Distribution of the normalized angular descriptor components  $\{q_{n4}\}_{n=1}^6$  (that is, most of the  $l = 4$  components) for the Pb and Te atoms in NEP1 and NEP2.

- 
- [1] Jörg Behler, “Perspective: Machine learning potentials for atomistic simulations,” *The Journal of Chemical Physics* **145**, 170901 (2016).
- [2] Volker L. Deringer, Miguel A. Caro, and Gábor Csányi, “Machine learning interatomic potentials as emerging tools for materials science,” *Advanced Materials* **31**, 1902765 (2019).
- [3] Tim Mueller, Alberto Hernandez, and Chuhong Wang, “Machine learning for interatomic potential models,” *The Journal of Chemical Physics* **152**, 050902 (2020).
- [4] Y. Mishin, “Machine-learning interatomic potentials for materials science,” *Acta Materialia* **214**, 116980 (2021).
- [5] Oliver T. Unke, Stefan Chmiela, Huziel E. Sauceda, Michael Gastegger, Igor Poltavsky, Kristof T. Schütt, Alexandre Tkatchenko, and Klaus-Robert Müller, “Machine learning force fields,” *Chemical Reviews* **121**, 10142–10186 (2021).
- [6] Jörg Behler and Michele Parrinello, “Generalized neural-network representation of high-dimensional potential-energy surfaces,” *Phys. Rev. Lett.* **98**, 146401 (2007).
- [7] Albert P. Bartók, Mike C. Payne, Risi Kondor, and Gábor Csányi, “Gaussian Approximation Potentials: The Accuracy of Quantum Mechanics, without the Electrons,” *Phys. Rev. Lett.* **104**, 136403 (2010).
- [8] A.P. Thompson, L.P. Swiler, C.R. Trott, S.M. Foiles, and G.J. Tucker, “Spectral neighbor analysis method for automated generation of quantum-accurate interatomic potentials,” *Journal of Computational Physics* **285**, 316–330 (2015).
- [9] Alexander V. Shapeev, “Moment tensor potentials: A class of systematically improvable interatomic potentials,” *Multiscale Modeling & Simulation* **14**, 1153–1173 (2016).
- [10] Han Wang, Linfeng Zhang, Jiequn Han, and Weinan E, “DeePMD-kit: A deep learning package for many-body potential energy representation and molecular dynamics,” *Computer Physics Communications* **228**, 178–184 (2018).
- [11] Linfeng Zhang, Jiequn Han, Han Wang, Roberto Car, and Weinan E, “Deep potential molecular dynamics: A scalable model with the accuracy of quantum mechanics,” *Phys. Rev. Lett.* **120**, 143001 (2018).
- [12] Kyuhyun Lee, Dongsun Yoo, Wonseok Jeong, and Seungwu Han, “SIMPLE-NN: An ef-

- cient package for training and executing neural-network interatomic potentials,” *Computer Physics Communications* **242**, 95–103 (2019).
- [13] Ruggero Lot, Franco Pellegrini, Yusuf Shaidu, and Emine Küçükbenli, “PANNA: Properties from Artificial Neural Network Architectures,” *Computer Physics Communications* **256**, 107402 (2020).
- [14] Xiang Gao, Farhad Ramezanghorbani, Olexandr Isayev, Justin S. Smith, and Adrian E. Roitberg, “TorchANI: A Free and Open Source PyTorch-Based Deep Learning Implementation of the ANI Neural Network Potentials,” *Journal of Chemical Information and Modeling* **60**, 3408–3417 (2020).
- [15] Yunqi Shao, Matti Hellström, Pavlin D. Mitev, Lisanne Knijff, and Chao Zhang, “PiNN: A Python Library for Building Atomic Neural Networks of Molecules and Materials,” *Journal of Chemical Information and Modeling* **60**, 1184–1192 (2020).
- [16] Punyaslok Pattnaik, Shampa Raghunathan, Tarun Kalluri, Prabhakar Bhimalapuram, C. V. Jawahar, and U. Deva Priyakumar, “Machine Learning for Accurate Force Calculations in Molecular Dynamics Simulations,” *The Journal of Physical Chemistry A* **124**, 6954–6967 (2020).
- [17] Howard Yanxon, David Zagaceta, Binh Tang, David S Matteson, and Qiang Zhu, “PyXtal\_FF: a python library for automated force field generation,” *Machine Learning: Science and Technology* **2**, 027001 (2021).
- [18] Yaolong Zhang, Junfan Xia, and Bin Jiang, “Physically Motivated Recursively Embedded Atom Neural Networks: Incorporating Local Completeness and Non-locality,” *Phys. Rev. Lett.* **127**, 156002 (2021).
- [19] Zheyong Fan, Zezhu Zeng, Cunzhi Zhang, Yanzhou Wang, Keke Song, Haikuan Dong, Yue Chen, and Tapio Ala-Nissila, “Neuroevolution machine learning potentials: Combining high accuracy and low cost in atomistic simulations and application to heat transport,” *Phys. Rev. B* **104**, 104309 (2021).
- [20] Tom Schaul, Tobias Glasmachers, and Jürgen Schmidhuber, “High dimensions and heavy tails for natural evolution strategies,” in *Proceedings of the 13th Annual Conference on Genetic and Evolutionary Computation* (Association for Computing Machinery, New York, NY, USA, 2011) pp. 845–852.
- [21] Daan Wierstra, Tom Schaul, Tobias Glasmachers, Yi Sun, Jan Peters, and Jürgen Schmidhuber, “Natural evolution strategies,” *Journal of Machine Learning Research* **15**, 949–980 (2014).
- [22] Zheyong Fan, Topi Siro, and Ari Harju, “Accelerated molecular dynamics force evaluation on graphics processing units for thermal conductivity calculations,” *Computer Physics Communications* **184**, 1414 – 1425 (2013).
- [23] Zheyong Fan, Wei Chen, Ville Vierimaa, and Ari Harju, “Efficient molecular dynamics simulations with many-body potentials on graphics processing units,” *Computer Physics Communications* **218**, 10 – 16 (2017). <https://github.com/brucefan1983/GPUMD>.
- [24] <https://github.com/libAtoms/QUIP>.
- [25] Ivan S Novikov, Konstantin Gubaev, Evgeny V Podryabinkin, and Alexander V Shapeev, “The MLIP package: moment tensor potentials with MPI and active learning,” *Machine Learning: Science and Technology* **2**, 025002 (2021).
- [26] Gastegger, L. Schwiedrzik, M. Bittermann, F. Berzsenyi, and P. Marquetand, “wACSF-Weighted atom-centered symmetry functions as descriptors in machine learning potentials,” *The Journal of Chemical Physics* **148**, 241709 (2018).
- [27] J. J. Artrith, Alexander Urban, and Gerbrand Ceder, “Efficient and accurate machine-learning interpolation of atomic energies in compositions with many species,” *Phys. Rev. B* **96**, 014112 (2017).
- [28] Konstantin Gubaev, Evgeny V. Podryabinkin, Gus L.W. Hart, and Alexander V. Shapeev, “Accelerating high-throughput searches for new alloys with active learning of interatomic potentials,” *Computational Materials Science* **156**, 148–156 (2019). <https://gitlab.com/brucefan1983/nep-data>.
- [29] V.I. Fedorov and V.I. Machuev, “Thermal Conductivity of PbTe, SnTe and GeTe in the solid and liquid phases,” *Sov. Phys. Solid State USSR* **11**, 1116 (1969).
- [30] A. A. El-Sharkawy, A. M. Abou El-Azm, M. I. Kenawy, A. S. Hillal, and H. M. Abu-Basha, “Thermophysical properties of polycrystalline PbS, PbSe, and PbTe in the temperature range 300–700 K,” *International Journal of Thermophysics* **4**, 261–269 (1983).
- [31] Zheyong Fan, Haikuan Dong, Ari Harju, and Tapio Ala-Nissila, “Homogeneous nonequilibrium molecular dynamics method for heat transport and spectral decomposition with many-body potentials,” *Phys. Rev. B* **99**, 064308 (2019).
- [32] Wanrun Jiang, Cunzhi Zhang, Linfeng Zhang, and Han Wang, “Accurate Deep Potential model for the Al-Cu-Mg alloy in the full concentration space,” *Chinese Physics B* **30**, 050706 (2021).
- [33] Denghui Lu, Wanrun Jiang, Yixiao Chen, Linfeng Zhang, Weile Jia, Han Wang, and Mohan Chen, “DP Train, then DP Compress: Model Compression in Deep Potential Molecular Dynamics,” (2021), [arXiv:2107.02103](https://arxiv.org/abs/2107.02103) [physics.comp-ph].